Biogeosciences Discuss., 12, 11113–11157, 2015
www.biogeosciences-discuss.net/12/11113/2015/
doi:10.5194/bgd-12-11113-2015

Biogeosciences Discussions
Open Access

The role of snow cover and soil freeze/thaw cycles affecting boreal-arctic soil carbon dynamics

Y. Yi[1], J. S. Kimball[1], M. A. Rawlins[2], M. Moghaddam[3], and E. S. Euskirchen[4]

[1]Numerical Terradynamic Simulation Group (NTSG), College of Forestry and Conservation, The University of Montana, MT, 59812, USA
[2]Department of Geosciences, University of Massachusetts, Amherst, MA, USA
[3]Department of Electrical Engineering, University of Southern California, CA, USA
[4]Institute of Arctic Biology, University of Alaska Fairbanks, Fairbanks, AK, USA

Received: 15 June 2015 – Accepted: 30 June 2015 – Published: 16 July 2015

Correspondence to: Y. Yi (yonghong.yi@ntsg.umt.edu)

Published by Copernicus Publications on behalf of the European Geosciences Union.

Abstract

Northern Hemisphere permafrost affected land areas contain about twice as much carbon as the global atmosphere. This vast carbon pool is vulnerable to accelerated losses through mobilization and decomposition under projected global warming. Satellite data records spanning the past 3 decades indicate widespread reductions (~ 0.8–1.3 days decade^{-1}) in the mean annual snow cover extent and frozen season duration across the pan-Arctic domain, coincident with regional climate warming trends. How the soil carbon pool responds to these changes will have a large impact on regional and global climate. Here, we developed a coupled terrestrial carbon and hydrology model framework with detailed 1-D soil heat transfer representation to investigate the sensitivity of soil organic carbon stocks and soil decomposition to changes in snow cover and soil freeze/thaw processes in the Pan-Arctic region over the past three decades (1982–2010). Our results indicate widespread soil active layer deepening across the pan-Arctic, with a mean decadal trend of 6.6 ± 12.0 (SD) cm, corresponding with widespread warming and lengthening non-frozen season. Warming promotes vegetation growth and soil heterotrophic respiration, particularly within surface soil layers (≤ 0.2 m). The model simulations also show that seasonal snow cover has a large impact on soil temperatures, whereby increases in snow cover promote deeper (≥ 0.5 m) soil layer warming and soil respiration, while inhibiting soil decomposition from surface (≤ 0.2 m) soil layers, especially in colder climate zones (mean annual $T \leq -10\,^{\circ}\mathrm{C}$). Our results demonstrate the important control of snow cover in affecting northern soil freeze/thaw and soil carbon decomposition processes, and the necessity of considering both warming, and changing precipitation and snow cover regimes in characterizing permafrost soil carbon dynamics.

BGD
12, 11113–11157, 2015

1 Introduction

The northern high latitudes contain about twice as much carbon as the global atmosphere, largely stored in permafrost and seasonally thawed soil active layers (Hugelius et al., 2014). This vast carbon pool is vulnerable to accelerated losses through mobilization and decomposition under regional warming, with potentially large global carbon and climate impacts (Koven et al., 2011; Schaefer et al., 2011; Schuur et al., 2015). The northern high latitudes have experienced a much stronger warming rate than the global average over recent decades (Serreze and Francis, 2006), and this warming trend is projected to continue, along with a general increase in surface precipitation (Solomon et al., 2007). A better understanding of how the northern soil carbon pool responds to these changes is critical to predict climate feedbacks and associated impacts to northern ecosystems.

Potential vulnerability of soil carbon to mobilization and accelerated decomposition with climate warming, particularly in permafrost areas, will largely depend on changes in soil moisture and thermal conditions (Grosse et al., 2011; Schaefer et al., 2011; Schuur et al., 2015). Widespread soil thawing and permafrost degradation in the boreal and Arctic have been reported (e.g. Jorgenson et al., 2006; Romanovsky et al., 2010a, b). This has triggered a series of changes in boreal and Arctic ecosystems, including changes in lake and wetland areas (Smith et al., 2005; Watts et al., 2012), tundra shrub cover expansion (Tape et al., 2006; Sturm et al., 2005), thermokarst and other disturbances (Grosse et al., 2011), which are likely having a profound influence on both surface and subsurface hydrology and biogeochemical cycles. In particular, increases in soil temperature and associated soil thawing potentially expose vast soil organic carbon stocks, formally stabilized in perennial frozen soils, to mobilization and decomposition, which may promote large positive climate feedbacks (Schaefer et al., 2011; Schuur et al., 2015).

Previous studies highlighted the importance of both surface air temperature and snow cover conditions affecting the soil thermal regime among many other factors

BGD
12, 11113–11157, 2015

(Stieglitz et al., 2003; Zhang, 2005; Osterkamp, 2007; Lawrence and Slater, 2010; Romanovsky et al., 2010a). Changes in the rate of accumulation, timing, duration, density and amount of snow cover during the winter season play an important role in determining how soil responds to surface warming due to strong insulation effects of snow cover on ground temperature and its role in the surface energy budget (Zhang, 2005). Both surface warming and a changing precipitation regime can modify seasonal snow cover conditions, leading to a non-linear soil response to warming (Lawrence and Slater, 2010). Increases in winter precipitation and deepening of the snowpack may enhance soil warming, while a reduced snowpack due to precipitation decreases or warming-enhanced snow sublimation may promote soil cooling. Changes in snow cover duration and condition can also alter the amount of energy absorbed by the ground and modify the rate of soil warming (Euskirchen et al., 2007). The Arctic is expected to experience continued warming and precipitation increases under projected climate trends (Solomon et al., 2007); how these climate trends will affect soil moisture and thermal dynamics is a key question affecting potential changes in northern soil carbon dynamics and associated climate feedbacks.

Satellite data records over the past three decades (1979–2011) indicate widespread reductions (~ 0.8–$1.3\,\text{days}\,\text{decade}^{-1}$) in mean annual snow cover extent and frozen season duration across the pan-Arctic domain, coincident with regional warming (Brown and Robinson, 2011; Kim et al., 2012). Earlier onset of spring snow melt and soil thaw has been observed from both in situ ground and satellite measurements, while the onset of snow cover and soil freezing in the fall show more variable trends (Brown and Robinson, 2011; Kim et al., 2012). More active snow melt during the snow season, largely in the early snow season, has also been observed from a passive microwave satellite remote sensing based freeze/thaw dataset (Kim et al., 2015). On the other hand, snow depth trends in the boreal/Arctic region show large spatial variability. For example, several studies have shown a general snow depth increase in eastern Siberia (e.g. Park et al., 2014) and decrease in western North America in recent decades (Dyer and Mote, 2006).

BGD
12, 11113–11157, 2015

The objective of this study is to assess how northern soil thermal and carbon dynamics respond to changes in surface temperature, snow cover and freeze/thaw conditions indicated by satellite observations. To that end, we developed a coupled hydrology and carbon model framework with detailed soil heat transfer representation adapted for the pan-Arctic basin and Alaska domain. We used this model to investigate recent climate-related impacts on soil thermal and carbon dynamics over the past three decades (1982–2010). We conducted a sensitivity analysis by running the model with different configurations of surface meteorology inputs to evaluate how soil thermal conditions and soil carbon dynamics respond to changes in air temperature and precipitation during the same period.

2 Methods

2.1 Model description

A coupled hydrology and carbon model was used to investigate sensitivity of the soil thermal regime and soil carbon decomposition to changes in surface air temperature and snow cover conditions. The hydrology model accounts for the effects of soil organic layers, changes in surface snow cover properties and soil water phase change on the soil freeze/thaw process in permafrost landscapes (Rawlins et al., 2013). These factors represent important controls on soil thermal dynamics within the active layer (Nicolsky et al., 2007; Lawrence and Slater, 2008, 2010), enabling improved estimation of subsurface soil temperature and moisture profiles, particularly in permafrost areas, and representation of essential environmental constraints on soil carbon decomposition (Yi et al., 2013).

The hydrology model used for this investigation is an extension of previous efforts on large-scale pan-Arctic water balance modeling (PWBM, Rawlins et al., 2003, 2013). Recent updates to the model include improved simulation of snow/ground and subsurface temperature dynamics using a 1-D heat transfer equation (Rawlins et al., 2013),

BGD
12, 11113–11157, 2015

instead of the empirical thaw depth estimation based on the Stefan solutions used in Rawlins et al. (2003). The updated PWBM model has 23 soil layers down to 60 m below surface, with increasing layer thickness at depth. Up to five snow layers are used to account for the effects of seasonal snow cover evolution on the ground thermal regime, and changes in seasonal snow density and thermal conductivities are also considered. Other model improvements include accounting for the impact of soil organic carbon content on soil thermal and hydraulic properties, an important feature of boreal and Arctic soils (Lawrence and Slater, 2008). Further details on the updated hydrology model are provided in Appendix A1.

A satellite-based terrestrial carbon flux (TCF) model (Yi et al., 2013) was coupled to the hydrology model for this investigation. The TCF model uses a light use efficiency algorithm driven by satellite estimates of FPAR (Fraction of vegetation canopy intercepted Photosynthetically Active Radiation) to estimate vegetation productivity and litterfall inputs to a soil decomposition model. In the original TCF model, soil carbon stocks and respiration fluxes were estimated using a simplified three-pool soil organic carbon (SOC) decomposition framework with environmental constraints on soil decomposition rates derived from either satellite-estimated surface soil moisture and temperature fields (Kimball et al., 2009) or reanalysis data (Yi et al., 2013). This approach assumes that the major source of soil heterotrophic respiration (R_h) comes from surface ($\leq$ 10 cm) litter and SOC layers. However, the contribution of deeper soils to total R_h may be non-negligible, especially in high latitude boreal and Arctic tundra landscapes with characteristic carbon-rich soils (Koven et al., 2011; Schuur et al., 2015). Therefore, in this study, we incorporated a more detailed soil decomposition model representing SOC stocks extending to 3 m below the surface, and representing differences in litterfall and soil organic matter substrate quality within the soil profile (Thornton et al., 2002). The resulting soil decomposition model used for this study includes three litterfall pools, three SOC pools with relatively fast turnover rates and a deep SOC pool with a slow turnover rate (Supplement Fig. S1). The three litterfall pools were distributed within the top 20 cm of the soil layers; the three fast SOC pools were distributed within the

BGD
12, 11113–11157, 2015

top 50 cm of the soil layers, and the deep SOC pool extended from 50 cm to 3 m below the surface, consistent with soil profile characteristics reported from regional field studies (Hugelius et al., 2014). Substantial SOC may be stored in permafrost soils below 3 m depth (Hugelius et al., 2014), and may potentially undergo mobilization with continued warming. However, this contribution to total land–atmosphere carbon (CO_2) exchange was assumed negligible for the recent historical period examined (Schaefer et al., 2011) and was not considered in this study. Further details on the carbon model used in this study are provided in Appendix A2.

2.2 Datasets

The modeling domain for this investigation encompasses the pan-Arctic drainage basin and Alaska, representing a total land area extent of approximately 24.95 million km^2 (Rawlins et al., 2013). The model was run at a 25 km Northern Hemisphere Equal-Area Scalable Earth Grid (EASE-Grid) spatial resolution and daily time step from 1979 to 2010. Further details on the model validation datasets and inputs used for this study are provided below.

2.2.1 In situ data

In situ measurements from 20 Eddy Covariance (EC) tower sites across the pan-Arctic domain were obtained from the La Thuile FLUXNET dataset (Baldocchi, 2008), and were used to evaluate the model simulated daily carbon fluxes, and soil temperature and moisture fields (Table S1 in the Supplement). The tower daily carbon flux estimates are derived from half-hourly EC CO_2 flux measurements that have been processed and aggregated using consistent gap filling and quality control procedures (Baldocchi, 2008). Limited surface ($\leq$ 15 cm) soil temperature and moisture measurements were also provided at a portion of the tower sites, but with unknown soil sampling depths and very few measurements at the tundra sites. Therefore, we selected one boreal

BGD
12, 11113–11157, 2015

forest and three tundra sites with detailed in situ measurements for additional model evaluation (Table 1).

The three tundra sites are located within the Imnavait Creek watershed in the northern foothills of the Brooks Range, Alaska (68°37′ N, 149°18′ W), and underlain with continuous permafrost (Euskirchen et al., 2012). Mean annual air temperature and precipitation at the site is −7.4 °C and 318 mm with about 40 and 60 % of annual precipitation occurring as rain and snow, respectively. There are three towers in three different tundra types, including dry heath, moist acidic tussock and wet sedge tundra. The surface soil organic layer thickness varies from 34.0 ± 2.4 cm in the wet sedge tundra to 2.3 ± 0.3 cm for dry heath tundra. The maximum active layer thaw depth varies from ∼ 40 cm at the dry heath site to ∼ 70 cm at the tussock tundra site (Euskirchen et al., 2012). Soil temperature and moisture at 5 cm depth were measured at each tundra site. All observations including carbon fluxes and soil temperature and moisture are available from 2008 to 2011.

The boreal forest site is part of a network of tower EC sites spanning a fire chronosequence in central Manitoba (55°54′ N, 98°31′ W) at various stages of succession following large stand replacement fires (Goulden et al., 2011). We chose one of the two oldest chronosequence tower sites burned in year 1930 for model validation because this site had more continuous measurements of carbon fluxes and surface meteorology, and high quality data (indicated by the tower metadata) during the observation period (2002–2005). This site is dominated by mature closed-canopy black spruce stands. The mean annual air temperature and precipitation at this site are −3.2 °C and 520 mm respectively. Soil temperatures were measured at the surface (0 cm) and at multiple (6, 11, 16, 18, 29, 41 and 55 cm) soil depths, while soil moisture was also measured at multiple (11, 18, 28, 41 and 55 cm) depths.

2.2.2 Model inputs

Primary model drivers include daily surface meteorology and satellite-based normalized difference vegetation index (NDVI) records. Daily average and minimum air tem-

BGD
12, 11113–11157, 2015

perature, precipitation, wind speed, atmosphere vapor pressure deficit (VPD) and downward solar radiation were obtained from a new version of the WATCH Forcing Data (WFD) applied to ERA-Interim reanalysis (WFDEI; Weedon et al., 2014). This dataset was created by extracting and interpolating the ERA-Interim reanalysis to $0.5^{\circ} \times 0.5^{\circ}$ spatial resolution with sequential elevation correction of surface meteorological variables and monthly bias correction from gridded observations including CRU TS (v3.1 and v3.2) and GPCC (v5 and v6) datasets (for precipitation only). The daily WFDEI surface meteorology data is available from 1979 to 2010 and allows more thorough comparisons of hydrological model outputs with other relevant satellite products than the previous WFD dataset (Weedon et al., 2014). The third-generation Global Inventory Monitoring and Modelling Studies (GIMMS3g) NDVI dataset (Xu et al., 2013) was used to estimate litterfall seasonality and FPAR, as critical inputs to the TCF model (Yi et al., 2013). The GIMMS3g dataset was assembled from different NOAA Advanced Very High Resolution Radiometer (AVHRR) sensor records, accounting for various deleterious effects including calibration loss, orbital drift and volcanic eruptions. The NDVI data has a 15 day temporal repeat and 8 km spatial resolution, extending from 1982 to 2010. For the model simulations, both WFDEI and GIMMS3g forcing datasets were re-gridded to a consistent 25 km EASE-GRID format and the bimonthly GIMMS3g data was interpolated to a daily time step. The NDVI data from year 1982 were used as drivers for model spin-up and simulations prior to the start of the GIMMS3g observation record (i.e. 1979–1981).

Other ancillary model inputs included a merged 8 km land cover dataset (Bi et al., 2013) combining the 500 m MODIS International Geosphere-Biosphere Programme (IGBP) land cover map (Friedl et al., 2010) and the Circumpolar Arctic Vegetation Map (CAVM; Walker et al., 2005). The CAVM was used to identify tundra vegetation within the circumpolar region as a supplement to the IGBP classification, which does not provide a specific category for tundra and forest-tundra transition biome types (Bi et al., 2013). The dominant land cover type within each 25 km EASE Grid cell was chosen based on the merged 8 km land cover dataset and reclassified according to the original

BGD
12, 11113–11157, 2015

PWBM land cover classification (Rawlins et al., 2013; Fig. S2). Tundra, forest-tundra and taiga/boreal biomes account for approximately 70 % of the total pan-Arctic drainage basin area (Fig. S2).

Soil organic carbon inventory data (GSDT, 2000; Hugelius et al., 2014) were used to prescribe the SOC fraction in each model soil layer. The fraction of SOC has a large impact on soil thermal and hydraulic properties, and is therefore an important control on characterizing soil freeze/thaw and moisture processes (Lawrence and Slater, 2008; Nicolsky et al., 2007). The IGBP Global Soil Data Task (GSDT, 2000) and the Northern Circumpolar Soil organic Carbon Database (NCSCD; Hugelius et al., 2014) SOC data was distributed through the top 11 model soil layers (≤ 1.4 m depth) across the study area following Rawlins et al. (2013) and Lawrence and Slater (2008). The NCSCD data, which provides an updated estimate of SOC in permafrost affected areas, was used to prescribe the SOC fraction for permafrost areas, while the GSDT data was applied to non-permafrost areas. Generally, the organic carbon fraction within the top 5 soil layers (≤ 23 cm depth) is high, with mean values of 53.7 and 39.4 % for the two deeper surface soil layers (13–23 cm depth) averaged over the pan-Arctic domain.

2.3 Model parameterization

A dynamic litterfall allocation scheme based on satellite NDVI data (Appendix A2) was used to prescribe the daily litterfall fraction through each annual cycle to account for litterfall seasonality, particularly for deciduous vegetation types (Randerson et al., 1996; White et al., 2000). The GIMMS3g NDVI bimonthly data was first aggregated to a monthly time step and then used to characterize monthly leaf loss and turnover rates of fine roots during the active growth period based on Eq. (A7). The monthly litterfall fraction was then evenly distributed on a daily time step within each month. This approach generally allocates more litterfall during the latter half of the growing season, while the model simulations show generally more soil heterotrophic respiration during the latter portion of the year (Fig. S3). A comparison of model simulations against tower measurements shows overall improved NEE seasonality relative to a previous

BGD
12, 11113–11157, 2015

TCF model application where litterfall was distributed evenly over the annual cycle (Yi et al., 2013).

2.4 Model sensitivity analysis

We conducted a model sensitivity analysis to examine how the estimated soil thermal regime and SOC decomposition respond to changes in surface air temperature and snow conditions over the satellite record extending from 1979 to 2010. Three sets of daily model simulations were run by: (1) varying air temperature (T) and precipitation (P) inputs, (2) varying T inputs alone (temperature sensitivity analysis), and (3) varying P inputs alone (precipitation sensitivity analysis). Daily mean T (including daily mean and minimum temperature) and P climatology was first derived from the initial three-year (1979–1981) WFDEI meteorological record and used in the model sensitivity runs. The daily climatology based on three-year (1979–1981) meteorological records rather than a single year (i.e. 1979) was used to minimize effects from characteristically large climate fluctuations in the northern high latitudes. For precipitation, we first created a monthly climatology from the daily record (1979–1981) and then scaled the daily WFDEI precipitation by maintaining the monthly climatology value (Lawrence and Slater, 2010):

$$P'(y,m,d) = \frac{\overline{P(m)}}{P(y,m)} P(y,m,d) \quad (1)$$

where y, m and d represent a particular year, month and day. $\overline{P(m)}$ is the precipitation monthly climatology averaged from 1979 to 1981 and $P(y,m)$ is the monthly total precipitation for a particular year and month. $P(y,m,d)$ and $P'(y,m,d)$ are the original and scaled daily precipitation for a particular year, month and day respectively. Due to a relatively short-period (i.e. 1979–1981) and large variability in northern latitude precipitation, the ratio of $\frac{\overline{P(m)}}{P(y,m)}$ may be too large for a particular month with extremely low

BGD
12, 11113–11157, 2015

precipitation rates. In this case, the daily precipitation was not adjusted to avoid unreasonable estimates. We then ran the model with different configurations of the daily surface meteorology datasets. Model simulations derived using the dynamic WFDEI daily surface meteorology from 1979 to 2010 (i.e. varying T and P) was used as the model baseline simulation. For the temperature sensitivity analysis, we ran the model using the dynamic daily WFDEI temperature records from 1979 to 2010, but holding P as the climatology value from 1979–1981. For the precipitation sensitivity analysis, we ran the model using the dynamic daily WFDEI precipitation records, but with the T daily climatology. Since VPD is dependent on air temperature, we also created a daily VPD climatology (1979–1981) as an additional input to the carbon model, assuming negligible changes in relative humidity during the study period for the precipitation sensitivity analysis. There was no significant trend in solar radiation during the study period; we therefore used the historical (i.e. 1979–2010) solar radiation data for the three sets of simulations.

The model was initialized using a two-step process prior to the three sets of simulations. The model was first spun-up using the daily surface climatology (1979–1981) including T, VPD, and P for 50 years to bring the top 3 m soil temperature into dynamic equilibrium; the model was then run using the same climatology and simulated soil temperature and moisture fields over several thousand years to bring the SOC pools to equilibrium. To reduce the impact of the spin-up on model simulations, we excluded the 1979 to 1981 period from our analysis.

3 Results

3.1 Model validation

The model was evaluated against 20 tower EC CO_2 flux measurement sites representing major vegetation types across the pan-Arctic domain, and having at least one year of observations available (Table 2). For the validation, the model was driven using tower

BGD
12, 11113–11157, 2015

observed meteorology. The model simulations were generally consistent with the tower measurement based carbon fluxes, with mean R values of 0.84±0.11 (SD) for gross primary production (GPP) and 0.63 ± 0.17 for net ecosystem exchange (NEE), and mean RMSE differences of 1.44 ± 0.50 gC m^{-2} day^{-1} for GPP and 1.04 ± 0.36 gC m^{-2} day^{-1} for NEE. The model results showed relatively large discrepancies with the tower based carbon fluxes for tundra sites; however, large uncertainties are associated with the tower measurements in tundra areas due to the characteristically harsh environment and extensive missing data. The simulated temperature and moisture fields also capture the seasonality of the in situ surface (≤ 15 cm) soil measurements representing variable soil depths (not shown), despite large uncertainties in the surface meteorology inputs (particularly precipitation/snowfall), and soil parameters including definition of texture and peat fraction within the soil profile. Additional assessment of the model simulations was conducted using detailed in situ measurements at selected tundra and boreal forest validation sites (Table 1) as summarized below.

The model simulations compared favourably with in situ measurements at the tundra validation sites for surface soil temperature (R = 0.93, RMSE = 3.12 °C) and carbon fluxes, including GPP (R = 0.72, RMSE = 0.76 gC m^{-2} day^{-1}) and NEE (R = 0.79, RMSE = 0.50 gC m^{-2} day^{-1}), but with relatively larger discrepancy during the winter when the model showed lower values of NEE (e.g., less CO_2 emissions) than the measurements (from December to February, DJF; Fig. 1). The simulated maximum soil thaw depth (~ 50 cm averaged from 2008 to 2011) was also consistent with site measurements, ranging from 40 to 70 cm at three locations within the tundra validation site (Euskirchen et al., 2012). An apparent cold bias ranging from −2 to −5 °C in the simulated soil temperature during the fall and winter period of year 2009 and 2010 (Fig. 1a) reflects lower model simulated snow depth and associated reductions in thermal buffering between the atmosphere and underlying soil layers. This cold bias in the simulated soil temperatures results in early freezing of simulated soil water content (Fig. S4). Compared with the tower observations, the simulated daily surface soil temperatures generally show large temporal variations, particularly during the summer (from June

BGD
12, 11113–11157, 2015

to August, JJA). There were also considerable differences among in situ soil temperatures at different tundra sites. Summer (JJA) soil temperature at the wet sedge tundra location was generally lower than the other tundra vegetation types, which may reflect higher soil water content and specific heat capacity, and greater latent heat loss from evapotranspiration, leading to slower soil warming at this site. Overall, the model simulations compare well with the tower observed carbon fluxes during the growing season, but significantly underestimate NEE and soil respiration during the dormant season. Model underestimation of soil respiration during the dormant season may reflect less liquid soil water represented by the model under frozen ($< 0\,^{\circ}C$) temperatures than the tower measurements (Fig. S4), and also lack of model representation of wind-induced CO_2 exchange between atmosphere and surface snow pack (Luers et al., 2014). The model generally shows earlier seasonal onset and offset of photosynthesis relative to the in situ measurements, while partitioning of the tower NEE measurements during the shoulder season may be subject to large uncertainties under partial snow cover conditions (Euskirchen et al., 2012).

The model simulations also compared favourably against observations at the boreal forest validation sites (Fig. 2), capturing observed seasonality in soil temperatures ($R > 0.95$, RMSE $< 2.00\,^{\circ}C$) at different soil depths, and against tower observed carbon fluxes for GPP ($R = 0.89$, RMSE $= 1.24\,gC\,m^{-2}\,day^{-1}$) and NEE ($R = 0.73$, RMSE $= 0.65\,gC\,m^{-2}\,day^{-1}$). Similar to the tundra sites, snow depth also has a large impact on simulated soil temperatures at the boreal forest sites, but subject to large uncertainties in both model snowfall inputs and forest canopy snow interception processes. The timing of simulated thaw and freeze of soil water at different depths is generally consistent with the tower measurements, with later seasonal thawing and freezing occurring in the deeper soils (Fig. S5). The tower site soil moisture measurements show larger variability than the model simulations during the growing season, which likely reflect differences in the model parameterization of surface moss/peat and mineral soil hydraulic conductivities relative to local site conditions. The model simulated NEE fluxes during the non-growing season stem mainly from soil heterotrophic

BGD
12, 11113–11157, 2015

respiration and are largely consistent with the in situ tower observations, generally diminishing towards the end of the year, and then gradually recovering with soil warming toward the onset of the growing season. Both the model and in situ tower NEE fluxes show large temporal variations during the growing season, largely due to GPP reduction caused by high vapour pressure deficit or water stress.

3.2 Climatic control on simulated permafrost and soil temperatures

The simulated permafrost area is generally consistent with previous estimates. The simulated mean permafrost area from 1982 to 2010 is approximately 11.3 million km^2, which is within the range of observation based estimates (11.2–13.5 million km^2) of the combined area for continuous (90–100 %) and discontinuous (50–90 %) permafrost extent over the northern polar region (≥ 45° N) (Zhang et al., 2000).

The simulated active layer depth (ALD) shows an overall increasing trend across the pan-Arctic domain over the 1982 to 2010 record (Fig. 3a and b). No strong bias was observed for the model ALD simulations compared against in situ observations for 53 pan-Arctic sites from the Circumpolar Active Layer Monitoring (CALM) program (Brown et al., 2000); these results showed a mean model bias of −9.48 cm, representing approximately 16.5 % of the estimated ALD, but with low model correspondence ($R = 0.31$, $p < 0.1$) in relation to the site observations (Fig. S6). This relatively large discrepancy between model simulated ALD results and in situ observations may be partly due to a spatial scale mismatch between the coarse resolution model simulations and the local in situ CALM site measurements, as well as uncertainties in the reanalysis surface meteorology data used as model forcings (Rawlins et al., 2013). Previous studies have shown large local spatial variations in ALD due to strong surface heterogeneity including microtopography, vegetation and soil moisture conditions (Romanovsky et al., 2010a, b). Simulated widespread ALD deepening is consistent with generally decreasing snow cover extent in the pan-Arctic region (Fig. 3c). Simulated ALD trends over the 1982–2010 record range from −4.32 to 8.05 cm yr^{-1}, with a mean value of 0.66 cm yr^{-1}. A notable ALD deepening trend occurs in discontinuous per-

BGD
12, 11113–11157, 2015

mafrost areas with relatively large mean ALD values. However, in portions of Alaska, the model simulations indicate slightly decreasing ALD trends across the study period (Fig. 3b), despite strong reduction in the local snow cover extent (Fig. 3c). This mainly reflects a large decrease in the simulated snowpack (Fig. 3d) due to a decreasing trend in WFDEI precipitation/snowfall data, resulting in less thermal insulation of underlying soil, which may offset warming effects from decreasing snow cover extent.

The regional differences in snow cover effects on model simulated ALD can be explained by different climatic controls on warm-season (May to October) soil temperatures. The correlation analysis between climate variables and warm-season soil temperatures (Fig. 4) indicate that surface warming has a dominant control on upper (< 0.5 m) soil temperatures in all climate zones, and also on deeper (≥ 0.5 m) soil temperatures in warmer climate zones (mean annual $T_{air} > -4\,^{\circ}C$). A deep snow pack has a strong warming effect on simulated deeper (≥ 0.5 m) soil temperatures in colder climate zones (mean annual $T_{air} \leq -4\,^{\circ}C$), but with limited warming effects on surface soil temperatures across all pan-Arctic climate zones. Correspondingly, the effects of seasonal snow cover duration on model soil temperatures vary across different climate zones and soil depths. In colder climate areas, a longer snow cover duration has a relatively strong warming effect on deeper (≥ 0.5 m) soil temperatures, but with negligible warming effects on the surface soil layers. In warmer areas, a shorter snow cover season promotes warmer soils, particularly within surface soil layers, due to stronger air and soil thermal coupling. Additional analysis also indicates that earlier snow cover seasonal onset in the fall has a stronger warming effect on modelled soil temperatures in colder climate areas, while earlier offset of seasonal snow cover in the spring has a stronger warming effect on modelled soil temperatures in the warmer climate areas.

3.3 Climatic control on simulated carbon fluxes

The model simulations indicated that air temperature has an overall dominant control on the two main components of the NEE flux (i.e. NPP and R_h) across all pan-Arctic climate zones, while snow has a larger control on estimated annual NEE fluxes in colder

BGD
12, 11113–11157, 2015

climate areas (Fig. 5). These results indicate that warming generally promotes vegetation photosynthesis and soil heterotrophic respiration in the pan-Arctic region. However, a reduced positive correlation between NPP and air temperature in warmer climate zones (mean $T_{air} > 0\,^{\circ}C$) also indicates that warming-induced drought may reduce vegetation productivity to some extent (Kim et al., 2012; Yi et al., 2014). No significant correlation ($p > 0.1$) between NEE and air temperature was observed for most areas (mean $T_{air} \leq 5\,^{\circ}C$) due to NEE being a residual between two large fluxes (i.e. NPP and R_h) with similar temperature responses. A predominantly positive correlation (mean $R = 0.32$; $p < 0.1$) between annual NEE and snow water equivalent (SWE) in colder regions (mean $T_{air} < -4\,^{\circ}C$) is mainly due to a strong positive correlation ($R > 0.60$, $p < 0.01$) between SWE and NEE fluxes during the cold season (November to April; Fig. S7). A deeper snow pack promotes warmer soil conditions (Fig. 4b) and associated SOC decomposition and heterotrophic respiration, which contributes significantly to annual NEE, especially in colder climate areas (Zimov et al., 1996). No significant correlation ($p > 0.1$) between annual snow cover extent (SCE) or SWE and warm-season (from May to October) carbon fluxes was observed.

While snow cover has a negligible effect on total estimated carbon fluxes during the warm season, it has a strong control on the composition of soil R_h (Fig. 6). An overall, deeper snow pack promotes model soil decomposition and respiration from deeper (≥ 0.5 m) soil layers, while inhibiting contributions from surface (≤ 0.2 m) soil layers, especially in colder climate areas. This response is due to a stronger warming effect of snow cover on deeper soil layers in colder areas (Fig. 4). Comparatively, even though air temperature has a strong control on total warm-season R_h fluxes, it has a limited effect on the contribution of different soil depths to total soil decomposition and respiration except in the warmer climate areas (mean annual $T_{air} > 0\,^{\circ}C$). In the cold season, a deeper snow pack also promotes soil decomposition in deeper (> 0.2 m) soil layers more than in surface (0–0.2 m) soil layers.

BGD
12, 11113–11157, 2015

3.4 Sensitivity of simulated soil thermal dynamics and soil carbon decomposition to climate variations

The model sensitivity analysis using different surface meteorology inputs indicated that warming and reduced snow cover extent promoted widespread ALD deepening across the pan-Arctic domain over the 1982 to 2010 record (Fig. 7). In Eurasia, strong winter warming reduced model simulated SWE and SCE, while increasing winter precipitation generally increased SWE and SCE. In North America, regional trends in winter snow pack and SCE were more variable due to variable trends in winter air temperature and precipitation. Therefore, the resulting model simulated trends in SWE and SCE based on varying temperature and precipitation inputs showed strong spatial heterogeneity across the pan-Arctic domain. The model sensitivity analysis based on varying temperature inputs alone indicated overall ALD deepening in permafrost areas, corresponding with widespread warming and reduced SCE. However, the sensitivity analysis based on varying precipitation alone showed more variable trends in the simulated ALD results. Areas with strong decreasing winter precipitation and snow pack trends, such as Interior Alaska and eastern Siberia, showed a decreasing ALD trend, attributed to reduced snow insulation effects. The results also indicated that changing air temperature had an overall dominant effect on the simulated ALD trends, though changing precipitation also contributed to ALD changes in some areas.

The model sensitivity analysis also indicated that varying precipitation accounts for more of the changes in the simulated R_h contribution from different soil depths (i.e., soil R_h ratio, Figs. 8, 9, and S8), which was consistent with the above results indicating strong control of snow cover on the soil R_h ratio at different soil depths. The model sensitivity results also indicated that changing air temperature had minimal impact on the simulated soil R_h ratio, while increasing (decreasing) winter snow pack in permafrost areas generally corresponded with increasing (decreasing) soil R_h ratio from deeper (> 0.5 m) soil layers and decreasing (increasing) soil R_h contributions from surface (0–0.2 m) soil layers (Fig. 8). This is particularly true in cold climate regions

BGD
12, 11113–11157, 2015

(mean annual $T_{air} < -10\,^{\circ}C$; Fig. 9). The simulated R_h ratio from the deeper soil layers (0.5–3.0 m) based on model runs using varying precipitation alone did not show significant difference ($p > 0.1$) from model simulations based on varying air temperature and precipitation. However, the simulated soil R_h ratio from both surface (0–0.2 m) and deeper (0.5–3.0 m) soil layers based on model runs using varying temperature alone was significantly ($p < 0.01$) different from model simulation results based on varying air temperature and precipitation. Moreover, cold regions (mean $T_{air} < -10\,^{\circ}C$) showed stronger decreasing trends in the R_h ratio from surface soil layers and increasing soil R_h contributions from deeper soil layers, likely due to increasing winter precipitation and snow cover (Figs. 7 and 8), and consistent with field studies involving snow cover manipulations and associated impacts on soil respiration (e.g. Nowinski et al., 2010).

4 Discussion

4.1 Impact of climate variations on soil active layer properties

Our results show that recent strong surface warming trends in the pan-Arctic region have promoted widespread soil thawing and active layer (ALD) deepening (Fig. 7), while changing precipitation and snow depth have had a relatively smaller impact on ALD trends (Figs. 4 and 7). We find a mean increasing ALD trend of $0.66 \pm 1.20\,cm\,yr^{-1}$ across the pan-Arctic region over the past three decades, which is similar to reported values from previous studies (Zhang et al., 2005; Romanovsky et al., 2010a), albeit representing different time periods. This overall ALD deepening trend across the pan-Arctic domain corresponds with widespread warming and warming-induced decreases in SCE (Fig. 3c), and increasing non-frozen season duration (Kim et al., 2012). Our analysis indicates that air temperature has a dominant control on upper (< 0.5 m) soil layer temperatures during the warm-season, with increasing control in warmer climate zones (Fig. 4a). The model simulations also suggest that most pan-Arctic permafrost areas, especially continuous permafrost areas, have a relatively shallow (< 1 m) active

BGD
12, 11113–11157, 2015

layer (e.g. Fig. 3a). Therefore, rapid warming of the upper soil layers corresponds with general ALD deepening.

Previous studies have also shown that summer air temperature is the primary control on ALD trends, while the relationship between snow cover and ALD is more variable (Zhang et al., 2005; Romanovsky et al., 2010a, b). Our results demonstrate that deeper snow pack conditions promote warming of deeper (> 0.5 m) soil layers, especially in colder climate regions of the domain (Fig. 4b), and this warming effect exceeds the impact of surface warming on the deeper soil layers (e.g. > 1 m). Previous studies indicate that changes in snow depth can influence borehole (10–20 m) permafrost temperatures as much as changes in air temperature (Stieglitz et al., 2003; Romanovsky et al., 2010a, b). Regional simulations from the improved Community Land Model (CLM) also indicate that snow state changes can explain 50 % or more of soil temperature trends at 1 m depth over the recent 50 year record (Lawrence and Slater, 2010). On the other hand, the impact of changing snow cover duration on soil temperatures may vary across different climate zones (Fig. 4c) due to the influence of both precipitation/snowfall and air temperature on snow cover duration. A shorter snow cover season may cool the soil in colder climate zones due to less insulation from cold temperatures, but may warm the soil in warmer climate zones by promoting greater atmospheric heat transfer into soils (Lawrence and Slater, 2010; Euskirchen et al., 2007). Our results indicate that recent regional trends toward continued warming, earlier spring snowmelt onset and a shorter snow cover season will likely enhance soil warming and permafrost degradation in relatively warmer (mean annual $T_{air} > -5\,^{\circ}C$) regions of the pan-Arctic domain.

4.2 Impact of climate variations on soil carbon dynamics

Snow cover is an important control on the annual carbon budget in cold regions (annual mean $T_{air} < -4\,^{\circ}C$; Fig. 5b and c), even though air temperature has a dominant control on both annual NPP and R_h fluxes across all climate zones (Fig. 5a). Strong snow cover insulation on soil temperature sustains soil respiration even under very

BGD
12, 11113–11157, 2015

cold winter air temperatures and the resulting winter soil respiration can be a large component of the annual NEE budget. Field experiments have shown that the winter soil respiration in tundra areas can offset total net carbon uptake during the growing season and thus switch the ecosystem from a net carbon sink to a carbon source (Zimov et al., 1996; Euskirchen et al., 2012; Luers et al., 2014). Our results also indicate the cold-season (November–April) R_h accounts for ~ 25 % of the annual total R_h for the whole pan-Arctic region, and this may be a conservative estimate since our model may underestimate soil respiration in tundra areas (Fig. 1b). The model simulations indicate very low (< 5 %) unfrozen water below ~ −3 °C at the tundra sites, while previous studies and the tower measurements (Fig. S4) indicate that substantial unfrozen water may remain even under very low soil temperatures (e.g. ~ −10 °C), sustaining soil microbial activities (Romanovsky and Osterkamp, 2000). All these studies highlight the importance of snow cover on the northern carbon cycle.

Even though air temperature has a dominant control on R_h during the warm season (from May to October), snow cover strongly influences the contribution of different soil depths to the total soil decomposition and R_h (Fig. 6). This non-linear response is due to different controls of surface air temperature and snow cover on soil temperatures at different soil depths (Zhang, 2005; Romanovsky et al., 2010a, b; Lawrence and Slater, 2010). Surface warming during the summer has a dominant control on upper soil layer temperatures (< 0.5 m; Fig. 4a), while a deeper winter snowpack has a persistent warming effect on deeper soil temperatures in colder climate areas (Fig. 4b). Therefore, surface warming likely promotes more heterotrophic respiration from surface litter and soil layers, while a deeper snow pack promotes soil respiration from deeper soil layers. This is particularly important for soil carbon dynamics in permafrost areas, where a large amount of soil carbon occurs in deep perennial frozen soils (Hugelius et al., 2014). Previous studies including field experiments have primarily focused on the effects of surface warming on permafrost soil carbon decomposition (e.g. Schuur et al., 2007; Koven et al., 2011; Schaefer et al., 2011), while our results show that snow cover may play a larger role than air temperature in influencing deeper soil tempera-

BGD
12, 11113–11157, 2015

tures and permafrost stability. This is also supported by a snow addition experiment in Alaska tundra areas (Nowinski et al., 2010), which showed that deep snow treatment resulted in a larger contribution of deep and old soil carbon decomposition to total soil heterotrophic respiration.

4.3 Limitations and uncertainties

A number of processes, notably fire disturbance, shrub expansion and thermokarst, are not included in this study but may be important factors affecting regional permafrost and soil carbon dynamics (Grosse et al., 2011; Schuur et al., 2015). A warming climate has been linked with increasing boreal-arctic fire activity and severity (Grosse et al., 2011). Fire can change the surface vegetation composition and consume a large portion of the soil organic layer, which can dramatically alter the surface energy balance and soil thermal properties, and cause rapid permafrost degradation (Harden et al., 2006; Jafarov et al., 2013). Both field experiments and satellite measurements indicate a "greening" Arctic with increasing shrub abundance due to climate warming (Tape et al., 2006). Shrub expansion in Arctic tundra can change the snow distribution and surface albedo, affecting the surface energy balance and underlying active layer and permafrost conditions (Sturm et al., 2005). Development of surface water ponding with thermokarst in ice-rich permafrost areas can alter the local surface hydrology, affecting permafrost and soil carbon decomposition (Schuur et al., 2007; Grosse et al., 2011).

Another important feature of the Arctic is strong surface heterogeneity, characterized by widespread lakes, ponds, wetlands and waterlogged soils as a result of both topography and restricted surface drainage due to underlying permafrost. Changes in both surface and subsurface hydrology are tightly coupled with local permafrost conditions and potential carbon and climate feedbacks (Smith et al., 2005; Watts et al., 2012; Yi et al., 2014; Schuur et al., 2015). Current large-scale model simulations, including this study, generally operate at coarse spatial resolutions (on the order of tens of kilometers or even larger), and may not adequately represent finer scale processes affecting surface hydrology and warming effects on active layer and permafrost processes

BGD
12, 11113–11157, 2015

(Koven et al., 2011; Schuur et al., 2015). Next generation satellites, including the NASA SMAP (Soil Moisture Active Passive) mission provide for finer-scale (i.e. 3–9 km resolution) monitoring and enhanced (L-band) microwave sensitivity to surface (∼< 5 cm) soil freeze/thaw and moisture conditions (Entekhabi et al., 2010), and likely enable improved regional hydrological and ecological model parameterizations and simulations that more accurately represent active layer conditions. Finer spatial scale observations using lower frequency (such as P-band) Synthetic Aperture Radar (SAR) measurements from airborne sensors such as AirMOSS (Tabatabaeenejad et al., 2015) may also provide improved information on sub-grid scale processes and subsurface soil thermal and moisture profiles, providing critical constraints on model predictions of soil active layer changes, and soil carbon and permafrost vulnerability.

5 Conclusions

We developed a coupled hydrology and terrestrial carbon flux modeling framework to evaluate the sensitivity of soil freeze/thaw conditions and soil carbon dynamics to recent climate variations across the pan-Arctic basin and Alaska during the past 3 decades (1982–2010). Our results indicate that surface warming promotes widespread soil thawing and active layer deepening due to strong control of surface air temperature on upper (< 0.5 m) soil temperatures during the warm season (from May to October). Recent trends indicating earlier spring snowmelt and shorter seasonal snow cover duration with regional warming (Dyer and Mote, 2006; Brown and Robinson, 2011; Kim et al., 2012) will mostly likely enhance soil warming in relatively warmer climate zones (mean annual T_{air} > −5 °C) and promote permafrost degradation in these areas. Even though air temperature has a dominant control on soil decomposition during the warm season, snow cover has a strong control on the contribution of different soil depths to the total soil heterotrophic respiration flux. A deeper snow pack inhibits surface (< 0.2 m) litter and soil organic carbon decomposition but enhances the soil decomposition and respiration from the deeper (> 0.5 m) soil carbon pool. This non-

BGD
12, 11113–11157, 2015

linear relationship between snow cover and soil decomposition is particularly important in permafrost areas, where a large amount of soil carbon is stored in deep perennial frozen soils that are potentially vulnerable to mobilization and accelerated losses from near-term climate change. Our results demonstrate the important control of snow cover in affecting northern soil freeze/thaw and soil carbon decomposition processes, and the necessity of considering both warming, and changing precipitation and snow cover regimes in characterizing permafrost soil carbon dynamics. In addition, further improvements to our capabilities for regional assessment and monitoring of precipitation and snow cover across the northern high latitudes are needed to improve quantification and understanding of linkages between snow and permafrost carbon dynamics.

Appendix A:

A1 Hydrology model description

The PWBM model (Rawlins et al., 2013) simulates snow and ground thermal dynamics by solving a 1-D heat transfer equation with phase change (Nicolsky et al., 2007):

$$C\frac{\partial}{\partial t}T(z,t) + L\zeta\frac{\partial}{\partial t}\theta(T,z) = \frac{\partial}{\partial z}\left(\lambda\frac{\partial}{\partial z}T(z,t)\right),$$
$$z \in [z_s, z_b] \quad \text{(A1)}$$

where $T(z,t)$ is the temperature (°C), $C(T,z)$ and $\lambda(T,z)$ are the volumetric heat capacity ($\mathrm{J\,m^{-3}\,K^{-1}}$) and thermal conductivity ($\mathrm{W\,m^{-1}\,K^{-1}}$) of soil respectively; L is the volumetric latent heat of fusion of water ($\mathrm{J\,m^{-3}}$); ζ is the volumetric water content, and θ is the unfrozen liquid water fraction. The Dirichlet boundary conditions at the snow/ground surface z_s, i.e., $T(z_s,t) = T_{air}(t)$, and a heat boundary condition at the lower boundary z_b, i.e., $\lambda\frac{\partial}{\partial z}T(l,t) = g$, were used to solve the heat equation, where T_{air} is the observed air temperature and g is the geothermal heat flux ($\mathrm{K\,m^{-1}}$). The volumetric water content (ζ) can be obtained by solving the Richard's equation. The unfrozen liquid water

BGD
12, 11113–11157, 2015

fraction (θ) was estimated empirically as:

$$\theta = \begin{cases} 1 & T \geq T_* \\ |T_*|^b |T|^{-b} & T < T_* \end{cases}. \quad \text{(A2)}$$

where the constant T_* is the freezing point depression, and b is a dimensionless parameter obtained from unfrozen water curve fitting (Romanovsky and Osterkamp, 2000).

The bulk thermal properties of soil (i.e. C and λ) are a combination of the thermal properties of soil solids, air, and thawed and frozen states of soil water (Rawlins et al., 2013). Particularly, for the soil solids, the volumetric heat capacity (C_s) and thermal conductivities (λ_s) vary with the fraction of organic carbon of the soil, defined as:

$$C_s = (1 - f)C_m + fC_o \quad \lambda_s = \lambda_m^{1-f} \lambda_o^f \quad \text{(A3)}$$

where f is the fraction of organic carbon in the soil, C_m and C_o are the volumetric heat capacities of the mineral and organic soils respectively, and λ_m and λ_o are the thermal conductivities of the mineral and organic soils respectively.

Up to five snow layers were used to characterize the snowpack dynamics and solve the snow temperature profile, with varying depth for each layer depending on the snow depth. A two-layer snow density model similar to Schaefer et al. (2009) was used to characterize the impact of the bottom depth hoar layer on the snow thermal conductivity for tundra and taiga, with fixed snow thermal conductivity for this layer. For the upper snow layer, both the snow heat capacity and thermal conductivity vary with snow density. Following Liston et al. (2007), temporal evolution of the snow density is mainly affected by new snowfall and compaction due to winds:

$$\frac{d\rho_s}{dt} = 0.1 a_1 U \rho_s e^{(-b(T_f - T_s))} e^{(-a_2 \rho_s)} \quad \text{(A4)}$$

where ρ_s is the snow density ($kg\,m^{-3}$), U represents the wind-speed contribution to the snow density changes with negligible influence for wind speed below $5\,m\,s^{-1}$; T_f

BGD
12, 11113–11157, 2015

and T_s are the freezing and snow temperatures, respectively; a_1, a_2 and b are empirical dimensionless parameters. The snow thermal conductivity (λ_{snow}) is an empirical estimate of snow density based on Sturm et al. (1997):

$$\lambda_{snow} = 0.138 - 1.01\rho_s + 3.233\rho_s^2 \quad \text{(A5)}$$

More details on the numerical solution of the heat transfer equation and the parametrization of the snow model can be found in Rawlins et al. (2013) and Nicolsky et al. (2007).

A2 Carbon model description

A satellite-based light use efficiency (LUE) approach was used to estimate vegetation productivity:

$$\mathrm{GPP} = \varepsilon \times \mathrm{FPAR} \times \mathrm{PAR} \quad \text{(A6)}$$

where GPP is the gross primary productivity ($\mathrm{gC\,m^{-2}\,day^{-1}}$); ε ($\mathrm{gC\,MJ^{-1}}$) is the LUE coefficient converting absorbed photosynthetically active solar radiation (APAR) to vegetation biomass, and FPAR defines the fraction of incident PAR ($\mathrm{MJ\,m^{-2}\,day^{-1}}$) absorbed by the vegetation canopy (i.e. APAR). A maximum LUE coefficient (ε_{mx}, $\mathrm{gC\,MJ^{-1}}$) was prescribed for each land cover type and was reduced for sub-optimal environmental conditions (including low air temperature, soil moisture and frozen conditions) to estimate ε (Yi et al., 2013). Vegetation net primary productivity (NPP) was estimated as a fixed portion of GPP for each biome type based on an assumption of conservatism in vegetation carbon use efficiency within similar plant functional types (Gifford, 2003).

A dynamic carbon allocation of litterfall estimated from NPP, based on Randerson et al. (1996) and White et al. (2000), was used to characterize litterfall seasonality. The total litterfall was partitioned into three components, including leaves, fine roots, and woody components with prescribed ratios for each plant functional type based on field experiments (White et al., 2000; Table S2). Daily constant turnover rates were prescribed for the woody components of litterfall including stems and coarse roots (White

BGD
12, 11113–11157, 2015

et al., 2000), while the NDVI time series were used to characterize turnover rates of the other two variable components of litterfall during leaf senescence and active growth periods (Randerson et al., 1996). Approximately half of the fine root turnover was assumed to occur during the active growing season, and the monthly variable fraction of litterfall was calculated as:

$$LT_{var1}(t) = \frac{LL(t)}{\sum_{t=1}^{12} LL(t)} \cdot (LT_{leaf} + LT_{froot} \cdot 0.5),$$

$$LT_{var2}(t) = \frac{NDVI(t)}{\sum_{t=1}^{12} NDVI(t)} \cdot LT_{froot} \cdot 0.5,$$

$$LL(t) = [0.5 \cdot NDVI(t-2) + NDVI(t-1)] - [NDVI(t+1) + 0.5 \cdot NDVI(t+2)] \quad \text{(A7)}$$

where $LT_{var1}(t)$ and $LT_{var2}(t)$ represent the litterfall fraction associated with leaf loss (i.e. $LL(t)$) and vegetation active growth, respectively; LT_{leaf} and LT_{froot} are the prescribed fractions of leaf and fine root components for each plant functional type, respectively (Table S2). The estimated monthly litterfall fraction was then distributed evenly within the month.

To account for the contribution of deep soil organic carbon pools to the total heterotrophic respiration (R_h), we extended the original Terrestrial Carbon Flux (TCF) soil decomposition model to incorporate soil organic carbon down to 3 m below surface, and multiple litter and soil organic carbon (SOC) pools were used to characterize the progressive decomposition of fresh litter to more recalcitrant materials. Following BIOME-BGC (Thornton et al., 2002), the new soil decomposition model includes 3 litter pools, 3 SOC pools with relatively fast turnover rates and a deep SOC pool with slow turnover rates (Fig. S1). The litterfall carbon inputs were first allocated to the 3 litter pools according to the substrate quality of each litterfall component, i.e. labile, cellulose and

BGD
12, 11113–11157, 2015

lignin fractions of estimated leaf, fine root, and woody litterfall (Table S3; White et al., 2000), and then transferred to the SOC pools through progressive decomposition.

For each carbon pool (C_i), the carbon balance of the decomposition process was defined as:

$$\frac{\partial C_i}{\partial t} = R_i + \sum_{j \neq i} (1 - r_j) T_{ji} k_j C_j - k_i C_i \quad \text{(A8)}$$

where R_i is the carbon input from litterfall allocated to pool i (only non-zero for the 3 litter pools), T_{ji} is the fraction of carbon directed from pool j to pool i with fraction r_j lost as respiration, and $k_i(k_j)$ is the decomposition rate of carbon pool $i(j)$. The heterotrophic respiration (R_h) is then computed as the sum of respiration fluxes from the decomposition process:

$$R_h = \sum_{i=1,7} r_i k_i C_i \quad \text{(A9)}$$

The soil decomposition rate (k_i) for each pool is derived as the product of a theoretical maximum rate constant ($k_{mx,i}$, Fig. S1) and dimensionless multipliers for soil temperature (T_{mult}) and moisture (W_{mult}) constraints to decomposition under prevailing climate conditions:

$$k_i = k_{mx,i} \cdot T_{mult} \cdot W_{mult} \quad \text{(A10)}$$

where T_{mult} and W_{mult} vary between 0 (fully constrained) and 1 (no constraint), as defined in Yi et al. (2013).

The Supplement related to this article is available online at doi:10.5194/bgd-12-11113-2015-supplement.

Acknowledgements. This work was supported with funding from the NASA Interdisciplinary Research in Earth Science program. Data from the Imnavait tundra tower measurement was collected through a grant from the National Science Foundation Office of Polar Programs, Arctic Observatory Network. We thank M. Goulden for providing boreal forest tower measurements in Manitoba, Canada.

BGD
12, 11113–11157, 2015

References

Baldocchi, D.: Breathing of the terrestrial biosphere: lessons learned from a global network of carbon dioxide flux measurement systems, Aust. J. Bot., 56, 1–26, 2008.

Bi, J., Xu, L., Samanta, A., Zhu, Z., and Myneni, R.: Divergent Arctic-boreal vegetation changes between North America and Eurasia over the past 30 years, Remote Sens., 5, 2093–2112, 2013.

Brown, J., Hinkel, K. M., and Nelson, F. E.: The Circumpolar Active Layer Monitoring (CALM) program: research designs and initial results, Polar Geography, 24, 166–258, 2000.

Brown, R. D. and Robinson, D. A.: Northern Hemisphere spring snow cover variability and change over 1922–2010 including an assessment of uncertainty, The Cryosphere, 5, 219–229, doi:10.5194/tc-5-219-2011, 2011.

Dyer, J. L. and Mote, T. L.: Spatial variability and trends in observed snow depth over North America, Geophys. Res. Lett., 33, L16503, doi:10.1029/2006GL027258, 2006.

Entekhabi, D., Njoku, E. G., O'Neill, P. E., Kellogg, K. H., Crow, W. T., Edelstein, W. N., Entin, J. K., Goodman, S. D., Jackson, T. J., Johnson, J., Kimball, J., Piepmeier, J. R., Koster, R. D., Martin, N., McDonald, K. C., Moghaddam, M., Moran, S., Reichle, R., Shi, J. C., Spencer, M. W., Thurman, S. W., Tsang, L., and Van Zyl, J.: The Soil Moisture Active Passive (SMAP) mission, P. IEEE, 98, 704–716, 2010.

Euskirchen, E. S., Mcguire, A. D., and Chapin, F. S.: Energy feedbacks of northern high-latitude ecosystems to the climate system due to reduced snow cover during 20th century warming, Glob. Change Biol., 13, 2425–2438, 2007.

Euskirchen, E. S., Bret-Harte, M. S., Scott, G. J., Edgar, C., and Shaver, G. R.: Seasonal patterns of carbon dioxide and water fluxes in three representative tundra ecosystems in northern Alaska, Ecosphere, 3, 4, doi:10.1890/es11-00202.1, 2012.

Friedl, M. A., Sulla-Menashe, D., Tan, B., Schneider, A., Ramankutty, N., Sibley, A., and Huang, X.: MODIS Collection 5 global land cover: algorithm refinements and characterization of new datasets, Remote Sens. Environ., 114, 168–182, 2010.

Gifford, R. M.: Plant respiration in productivity models: conceptualisation, representation and issues for global terrestrial carbon-cycle research, Funct. Plant Biol., 30, 171–186, 2003.

Global Soil Data Task: 2000, Global Soil Data Products CD-ROM (IGBP-DIS), CD-ROM, International Geosphere-Biosphere Programme, Data and Information System, Potsdam, Ger-

BGD
12, 11113–11157, 2015

many, Available from Oak Ridge National Laboratory Distributed Active Archive Center, Oak Ridge, Tennessee, USA.

Goulden, M. L., McMillan, A. M. S., Winston, G. C., Rocha, A. V., Manies, K. L., Harden, J. W., and Bond-Lamberty, B. P.: Patterns of NPP, GPP, respiration, and NEP during boreal forest succession, Glob. Change Biol., 17, 855–871, 2011.

Grosse, G., Harden, J., Turetsky, M., McGuire, A. D., Camill, P., Tarnocai, C., Frolking, S., Schuur, E. A. G., Jorgenson, T., Marchenko, S., Romanovsky, V., Wickland, K. P., French, N., Waldrop, M., Bourgeau-Chavez, L., and Striegl, R. G.: Vulnerability of high-latitude soil organic carbon in North America to disturbance, J. Geophys. Res., 116, G00K06, doi:10.1029/2010JG001507, 2011.

Harden, J. W., Manies, K. L., Turetsky, M. R., and Neff, J. C.: Effects of wildfire and permafrost on soil organic matter and soil climate in interior Alaska, Glob. Change Biol., 12, 2391–2403, 2006.

Hugelius, G., Strauss, J., Zubrzycki, S., Harden, J. W., Schuur, E. A. G., Ping, C.-L., Schirrmeister, L., Grosse, G., Michaelson, G. J., Koven, C. D., O'Donnell, J. A., Elberling, B., Mishra, U., Camill, P., Yu, Z., Palmtag, J., and Kuhry, P.: Estimated stocks of circumpolar permafrost carbon with quantified uncertainty ranges and identified data gaps, Biogeosciences, 11, 6573–6593, doi:10.5194/bg-11-6573-2014, 2014.

Jorgenson, M. T., Shur, Y. L., and Pullman, E. R.: Abrupt increase in permafrost degradation in Arctic Alaska, Geophys. Res. Lett., 33, L02503, doi:10.1029/2005GL024960, 2006.

Kim, Y., Kimball, J. S., Zhang, K., and McDonald, K. C.: Satellite detection of increasing Northern Hemisphere non-frozen seasons from 1979 to 2008: implications for regional vegetation growth, Remote Sens. Environ., 121, 472–487, 2012.

Kim, Y., Kimball, J. S., Robinson, D. A., and Derksen, C.: New satellite climate data records indicate strong coupling between recent frozen season changes and snow cover over high northern latitudes, Environ. Res. Lett., in press, 2015.

Kimball, J. S., Jones, L. A., Zhang, K., Heinsch, F. A., McDonald, K. C., and Oechel, W. C.: A satellite approach to estimate land–atmosphere CO_2 exchange for Boreal and Arctic biomes using MODIS and AMSR-E, IEEE T. Geosci. Remote, 47, 569–587, 2009.

Koven, C. D., Ringeval, B., Friedlingstein, P., Ciais, P., Cadule, P., Khvorostyanov, D., Krinner, G., and Tarnocai, C.: Permafrost carbon-climate feedbacks accelerate global warming, P. Natl. Acad. Sci. USA, 108, 14769–14774, 2011.

BGD
12, 11113–11157, 2015

Jafarov, E. E., Romanovsky, V. E., Genet, H., McGuire, A. D., and Marchenko, S. S.: The effects of fire on the thermal stability of permafrost in lowland and upland black spruce forests of interior Alaska in a changing climate, Environ. Res. Lett., 8, 035030, doi:10.1088/1748-9326/8/3/035030, 2013.

Lawrence, D. M. and Slater, A. G.: Incorporating organic soil into a global climate model, Clim. Dynam., 30, 145–160, 2008.

Lawrence, D. M. and Slater, A. G.: The contribution of snow condition trends to future ground climate, Clim. Dynam., 34, 969–981, 2010.

Liston, G. E., Haehnel, R. B., Sturm, M., Hiemstra, C. A., Berezovskaya, S., and Tabler, R. D.: Instruments and methods simulating complex snow distributions in windy environments using SnowTran-3D, J. Glaciol., 53, 241–256, 2007.

Lüers, J., Westermann, S., Piel, K., and Boike, J.: Annual CO_2 budget and seasonal CO_2 exchange signals at a high Arctic permafrost site on Spitsbergen, Svalbard archipelago, Biogeosciences, 11, 6307–6322, doi:10.5194/bg-11-6307-2014, 2014.

Nicolsky, D. J., Romanovsky, V. E., Alexeev, V. A., and Lawrence, D. M.: Improved modeling of permafrost dynamics in a GCM land-surface scheme, Geophys. Res. Lett., 34, L08501, doi:10.1029/2007GL029525, 2007.

Nowinski, N. S., Taneva, L., Trumbore, S. E., and Welker, J. M.: Decomposition of old organic matter as a result of deeper active layers in a snow depth manipulation experiment, Oecologia, 163, 785–792, 2010.

Osterkamp, T. E.: Characteristics of the recent warming of permafrost in Alaska, J. Geophys. Res.-Earth, 112, F02S02, doi:10.1029/2006JF000578, 2007.

Park, H., Sherstiukov, A. B., Fedorov, A. N., Polyakov, I. V., and Walsh, J. E.: An observation-based assessment of the influences of air temperature and snow depth on soil temperature in Russia, Environ. Res. Lett., 9, 064026, doi:10.1088/1748-9326/9/6/064026, 2014.

Randerson, J. T., Thompson, M. V., Malmstrom, C. M., Field, C. B., and Fung, I. Y.: Substrate limitations for heterotrophs: implications for models that estimate the seasonal cycle of atmospheric CO_2, Global Biogeochem. Cy., 10, 585–602, 1996.

Rawlins, M. A., Lammers, R. B., Frolking, S., Fekete, B. Z. M., and Vorosmarty, C. J.: Simulating pan-Arctic runoff with a macro-scale terrestrial water balance model, Hydrol. Process., 17, 2521–2539, 2003.

BGD
12, 11113–11157, 2015

Rawlins, M. A., Nicolsky, D. J., McDonald, K. C., and Romanovsky, V. E.: Simulating soil freeze/thaw dynamics with an improved pan-Arctic water balance model, Journal of Advances in Modeling Earth Systems, 5, 659–675, 2013.

Romanovsky, V. E. and Osterkamp, T. E.: Effects of unfrozen water on heat and mass transport processes in the active layer and permafrost, Permafrost Periglac., 11, 219–239, 2000.

Romanovsky, V. E., Drozdov, D. S., Oberman, N. G., Malkova, G. V., Kholodov, A. L., Marchenko, S. S., Moskalenko, N. G., Sergeev, D. O., Ukraintseva, N. G., Abramov, A. A., Gilichinsky, D. A., and Vasiliev, A. A.: Thermal state of permafrost in Russia, Permafrost Periglac., 21, 136–155, 2010a.

Romanovsky, V. E., Smith, S. L., and Christiansen, H. H.: Permafrost thermal state in the polar Northern Hemisphere during the international polar year 2007–2009: a synthesis, Permafrost Periglac., 21, 106–116, 2010b.

Schaefer, K., Zhang, T. J., Slater, A. G., Lu, L. X., Etringer, A., and Baker, I.: Improving simulated soil temperatures and soil freeze/thaw at high-latitude regions in the Simple Biosphere/Carnegie-Ames-Stanford Approach model, J. Geophys. Res.-Earth, 114, F02021, doi:10.1029/2008JF001125, 2009.

Schaefer, K., Zhang, T. J., Bruhwiler, L., and Barrett, A. P.: Amount and timing of permafrost carbon release in response to climate warming, Tellus B, 63, 165–180, 2011.

Schuur, E. A. G., Crummer, K. G., Vogel, J. G., and Mack, M. C.: Plant species composition and productivity following permafrost thaw and thermokarst in alaskan tundra, Ecosystems, 10, 280–292, 2007.

Schuur, E. A. G., McGuire, A. D., Schädel, C., Grosse, G., Harden, J. W., Hayes, D. J., Hugelius, G., Koven, C. D., Kuhry, P., Lawrence, D. M., Natali, S. M., Olefeldt, D., Romanovsky, V. E., Schaefer, K., Turetsky, M. R., Treat, C. C., and Vonk, J. E.: Climate change and the permafrost carbon feedback, Nature, 520, 171–179, 2015.

Serreze, M. C. and Francis, J. A.: The arctic amplification debate, Climatic Change, 76, 241–264, 2006.

Smith, L. C., Sheng, Y., MacDonald, G. M., and Hinzman, L. D.: Disappearing Arctic lakes, Science, 308, 1429–1429, 2005.

Solomon, S.: Intergovernmental Panel on Climate Change and Intergovernmental Panel on Climate Change, Working Group I: Climate Change 2007: The Physical Science Basis: Contribution of Working Group I to the Fourth Assessment Report of the Intergovernmental Panel on Climate Change, Cambridge University Press, Cambridge, New York, 2007.

BGD
12, 11113–11157, 2015

Stieglitz, M.: The role of snow cover in the warming of arctic permafrost, Geophys. Res. Lett., 30, 1721, doi:10.1029/2003GL017337, 2003.
Sturm, M., Holmgren, J., Konig, M., and Morris, K.: The thermal conductivity of seasonal snow, J. Glaciol., 43, 26–41, 1997.
Sturm, M., Schimel, J., Michaelson, G., Welker, J. M., Oberbauer, S. F., Liston, G. E., Fahnestock, J., and Romanovsky, V. E.: Winter biological processes could help convert arctic tundra to shrubland, Bioscience, 55, 17–26, 2005.
Tabatabaeenejad, A., Burgin, M., Duan, X. Y., and Moghaddam, M.: P-band radar retrieval of subsurface soil moisture profile as a second-order polynomial: first AirMOSS results, IEEE T. Geosci. Remote, 53, 645–658, 2015.
Tape, K., Sturm, M., and Racine, C.: The evidence for shrub expansion in Northern Alaska and the pan-Arctic, Glob. Change Biol., 12, 686–702, 2006.
Thornton, P. E., Law, B. E., Gholz, H. L., Clark, K. L., Falge, E., Ellsworth, D. S., Golstein, A. H., Monson, R. K., Hollinger, D., Falk, M., Chen, J., and Sparks, J. P.: Modeling and measuring the effects of disturbance history and climate on carbon and water budgets in evergreen needleleaf forests, Agr. Forest Meteorol., 113, 185–222, 2002.
Walker, D. A., Raynolds, M. K., Daniels, F. J. A., Einarsson, E., Elvebakk, A., Gould, W. A., Katenin, A. E., Kholod, S. S., Markon, C. J., Melnikov, E. S., Moskalenko, N. G., Talbot, S. S., Yurtsev, B. A., and Team, C.: The Circumpolar Arctic vegetation map, J. Veg. Sci., 16, 267–282, 2005.
Watts, J. D., Kimball, J. S., Jones, L. A., Schroeder, R., and McDonald, K. C.: Satellite microwave remote sensing of contrasting surface water inundation changes within the Arctic-Boreal region, Remote Sens. Environ., 127, 223–236, 2012.
Weedon, G. P., Balsamo, G., Bellouin, N., Gomes, S., Best, M. J., and Viterbo, P.: The WFDEI meteorological forcing data set: WATCH Forcing Data methodology applied to ERA-Interim reanalysis data, Water Resour. Res., 50, 7505–7514, 2014.
White, M. A., Thornton, P. E., Running, S. W., and Nemani, R. R.: Parameterization and sensitivity analysis of the BIOME–BGC Terrestrial Ecosystem Model: net primary production controls, Earth Interact., 4, 1–85, 2000.
Xu, L., Myneni, R. B., Chapin III, F. S., Callaghan, T. V., Pinzon, J. E., Tucker, C. J., Zhu, Z., Bi, J., Ciais, P., Tømmervik, H., Euskirchen, E. S., Forbes, B. C., Piao, S. L., Anderson, B. T., Ganguly, S., Nemani, R. R., Goetz, S. J., Beck, P. S. A., Bunn, A. G., Cao, C., and Stroeve, J. C.:

BGD
12, 11113–11157, 2015

Temperature and vegetation seasonality diminishment over northern lands, Nature Climate Change, 581–586, doi:10.1038/nclimate1836, 2013.

Yi, Y., Kimball, J. S., Jones, L. A., Reichle, R. H., Nemani, R., and Margolis, H. A.: Recent climate and fire disturbance impacts on boreal and arctic ecosystem productivity estimated using a satellite-based terrestrial carbon flux model, J. Geophys. Res.-Biogeo., 118, 606–622, 2013.

Yi, Y., Kimball, J. S., and Reichle, R. H.: Spring hydrology determines summer net carbon uptake in northern ecosystems, Environ. Res. Lett., 9, 064003, doi:10.1088/1748-9326/9/6/064003, 2014.

Zhang, T.: Influence of the seasonal snow cover on the ground thermal regime: an overview, Rev. Geophys., 43, RG4002, doi:10.1029/2004RG000157, 2005.

Zhang, T., Heginbottom, J. A., Barry, R. G., and Brown, J.: Further statistics on the distribution of permafrost and ground ice in the Northern Hemisphere, Polar Geography, 24, 126–131, 2000.

Zhang, T., Frauenfeld, O. W., Serreze, M. C., Etringer, A., Oelke, C., McCreight, J., Barry, R. G., Gilichinsky, D., Yang, D. Q., Ye, H. C., Ling, F., and Chudinova, S.: Spatial and temporal variability in active layer thickness over the Russian Arctic drainage basin, J. Geophys. Res.-Atmos., 110, D16101, doi:10.1029/2004JD005642, 2005.

Zimov, S. A., Davidov, S. P., Voropaev, Y. V., Prosiannikov, S. F., Semiletov, I. P., Chapin, M. C., and Chapin, F. S.: Siberian CO_2 efflux in winter as a CO_2 source and cause of seasonality in atmospheric CO_2, Climatic Change, 33, 111–120, 1996.

BGD
12, 11113–11157, 2015

Table 1. Characteristics of two selected tundra and boreal forest tower sites used for model validation. Three tundra types are represented by the tower measurements at Imnavait Creek, Alaska, including dry heath, moist acidic tussock and wet sedge tundra. The boreal forest site encompasses a set of tower Eddy Covariance (EC) sites and measurements spanning a regional fire chronosequence at various succession stages in central Manitoba, Canada.

	Tundra	Boreal forest
Site	Imnavait Creek, Alaska	Manitoba, Canada
Location (Lat, Lon)	68°37′ N, 149°18′ W	55°54′ N, 98°31′ W
Permafrost	Continuous permafrost	No
Observation period	2008–2011	2002–2005
Soil temperature measurement depths (cm)	0, 5	0, 6, 11, 16, 18, 29, 41, 55
Soil moisture measurements depths (cm)	5	11, 18, 28, 41, 55

BGD
12, 11113–11157, 2015

Table 2. Correlations (R) and root mean square error (RMSE) differences between model simulated daily carbon fluxes and in situ tower eddy covariance measurement based observations across the study area.

PFT	Tower sites	GPP_R	GPP_RMSE ($gC\,m^{-2}\,day^{-1}$)	NEE_R	NEE_RMSE ($gC\,m^{-2}\,day^{-1}$)
ENF	12	0.83 ± 0.12	1.46 ± 0.59	0.56 ± 0.15	1.06 ± 0.40
DBF	2	0.91 ± 0.01	1.31 ± 0.60	0.77 ± 0.02	1.29 ± 0.39
MXF	3	0.88 ± 0.02	1.46 ± 0.45	0.76 ± 0.07	1.00 ± 0.29
GRS	1	0.92	1.38	0.89	1.12
WET	1	0.83	1.23	0.71	0.75
Tundra	1	0.62	1.76	0.38	0.66

PFT (plant function type): ENF: evergreen needle-leaf forest; DBF: deciduous broadleaf forest; MXF: mixed forest; GRS: grassland; WET: wetland.

BGD
12, 11113–11157, 2015

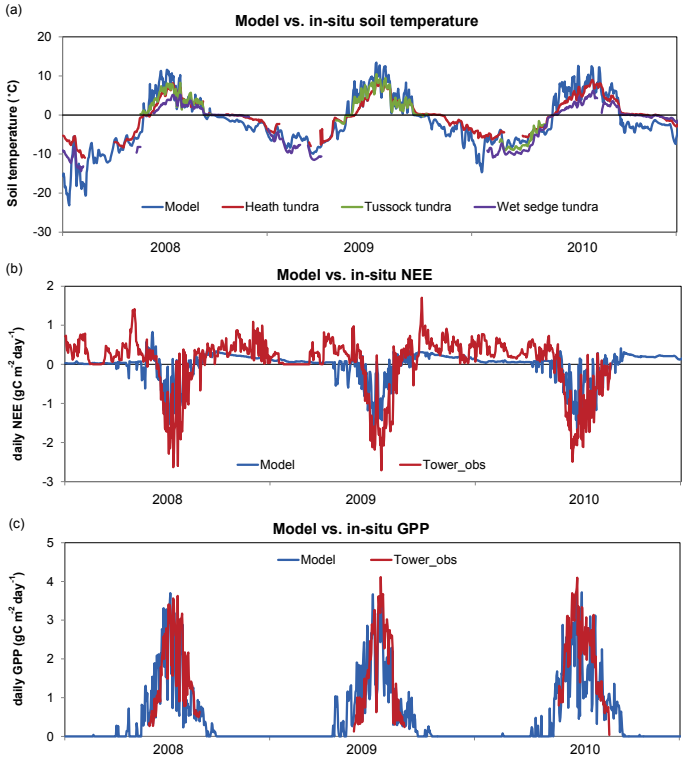

Figure 1. Comparisons of model simulated **(a)** surface soil temperature (~ 5 cm depth) and carbon fluxes (**b**: NEE and **c**: GPP), and tower measurements at the Imnavait Creek, Alaska tundra sites, over a three year (2008–2010) daily record. The tower observed carbon fluxes were averaged across three tundra vegetation types, including dry heath, moist acidic tussock and wet sedge tundra. NEE measurements were not collected at the tussock tundra site during the winter; therefore, the winter NEE measurements were averaged for the dry heath and wet sedge tundra sites only.

BGD
12, 11113–11157, 2015

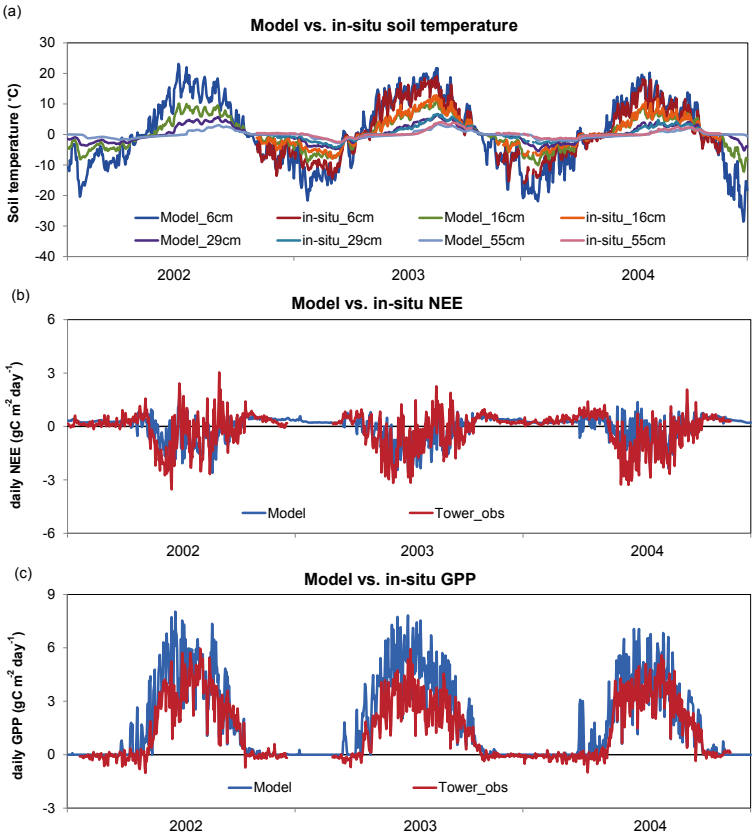

Figure 2. Comparisons of model simulated **(a)** soil temperature at different depths (6, 16, 29, and 55 cm) and carbon fluxes (**b**: NEE and **c**: GPP), and tower measurements at a mature boreal forest site in Manitoba, Canada over a three year (2002–2004) daily record.

BGD
12, 11113–11157, 2015

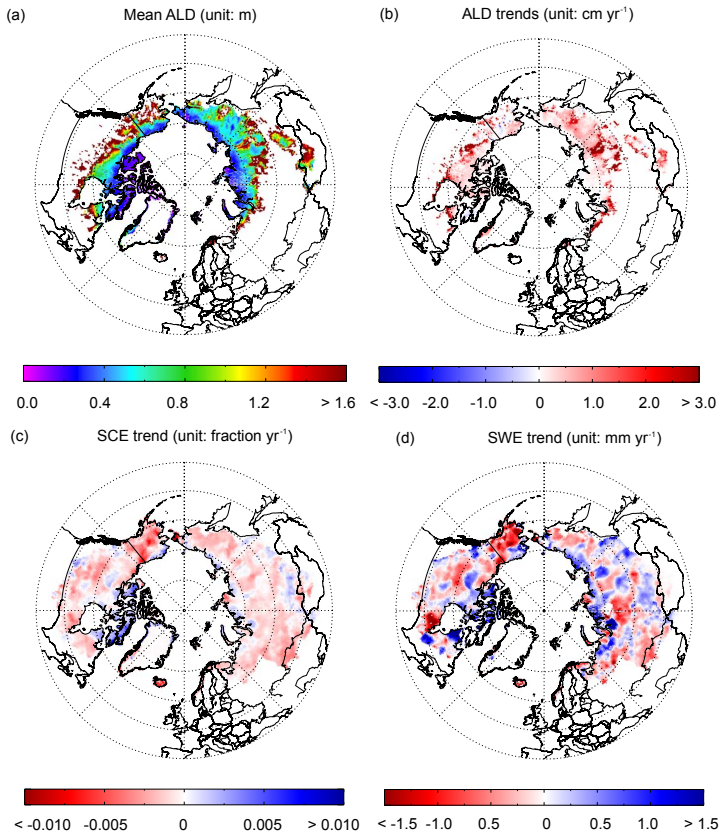

Figure 3. Model simulated spatial pattern of active layer depth (ALD, **a**) and estimated trends in ALD **(b)**, snow cover extent (SCE, **c**) and snow water equivalent (SWE, **d**) over the pan-Arctic basin and Alaska domain from 1982 to 2010. Areas in white are non-permafrost areas **(a, b)** or outside of the modeling domain.

BGD
12, 11113–11157, 2015

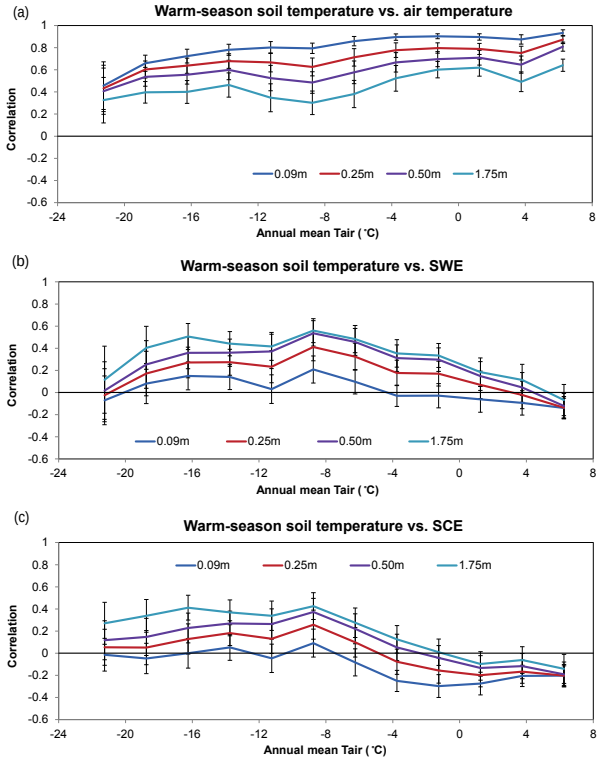

Figure 4. Correlations between climate variables and warm-season (May–October) soil temperature at different soil depths (0.09, 0.25, 0.50 and 1.75 m). The climate variables include warm-season air temperature (T_{air}), preseason snow water equivalent (SWE) and snow cover extent (SCE). The preseason is defined from November of the previous year to April of this year. The correlations were binned into 2.5 °C intervals. The standard deviation of correlations across each climate zone is shown through the error bars.

BGD
12, 11113–11157, 2015

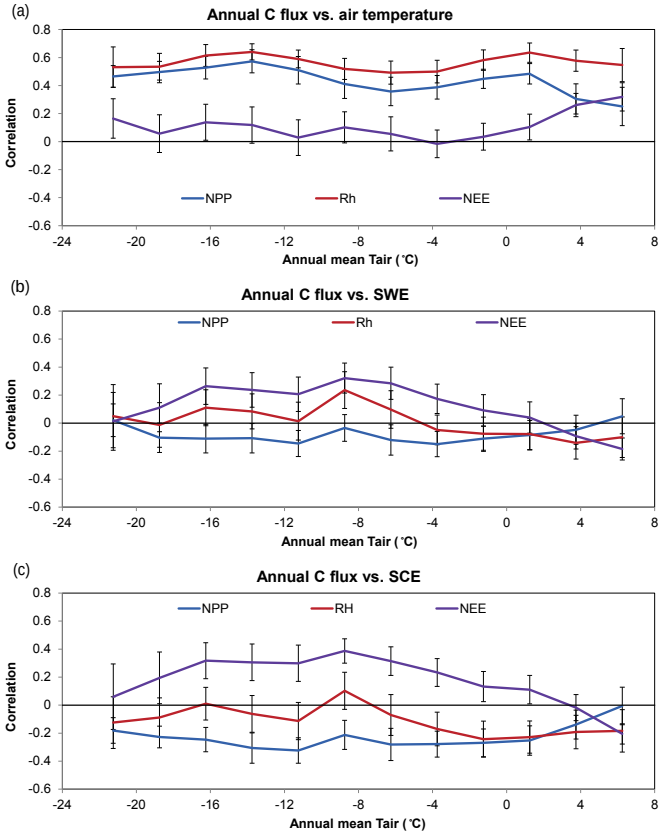

Figure 5. Correlations between climate variables and annual carbon fluxes. The climate variables include annual mean air temperature (T_{air}), snow water equivalent (SWE) and snow cover extent (SCE). The annual carbon fluxes include NEE and its two component fluxes (i.e. NPP and soil heterotrophic respiration R_h). The correlations were binned into 2.5°C intervals. The standard deviation of correlations across each climate zone is shown through the error bars.

BGD
12, 11113–11157, 2015

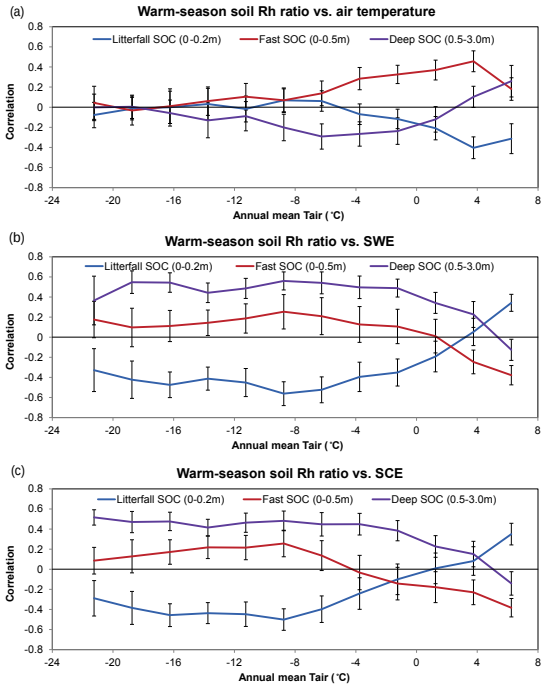

Figure 6. Correlations between climate variables and warm-season (May–October) soil heterotrophic respiration (R_h) composition from soil organic carbon (SOC) pools distributed at different soil depths (i.e. R_h ratio). The climate variables include warm-season air temperature (T_{air}), preseason snow water equivalent (SWE) and snow cover extent (SCE). The correlations were binned into 2.5 °C intervals. The 3 litterfall SOC pools were distributed at the top 0.2 m of the soil layers, the 3 SOC pools with fast turnover rates were distributed at the top 0.5 m of the soil layers, and the deep SOC pool with slow turnover rates was extending from the 0.5 to 3 m below surface. The standard deviation of correlations across each climate zone is shown through the error bars.

BGD
12, 11113–11157, 2015

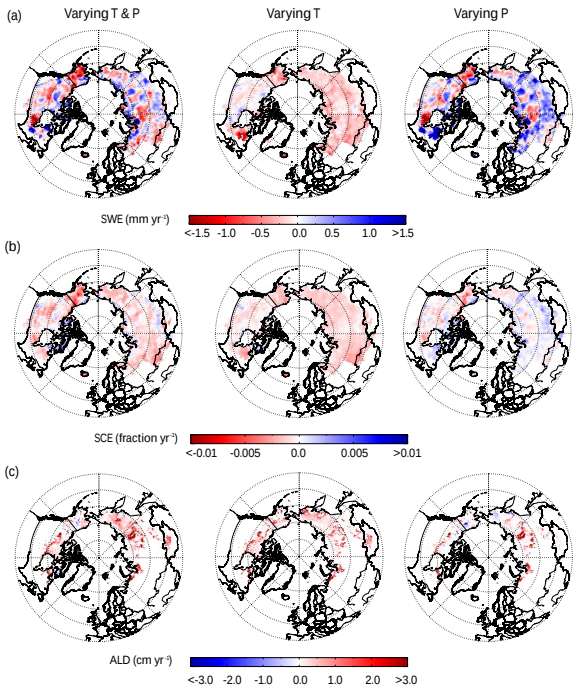

Figure 7. Simulated trends of snow water equivalent (SWE), snow cover extent (SCE) and active layer depth (ALD) for the three model sensitivity experiments for the 1982 to 2010 period. For the sensitivity analysis, the model was driven using different surface meteorology datasets. The results based on model runs using varying temperature (T) and precipitation (P) are presented in the left column; the results based on model runs using varying T alone are shown in the middle column, and results based on model runs using varying P alone are shown in the right column.

BGD
12, 11113–11157, 2015

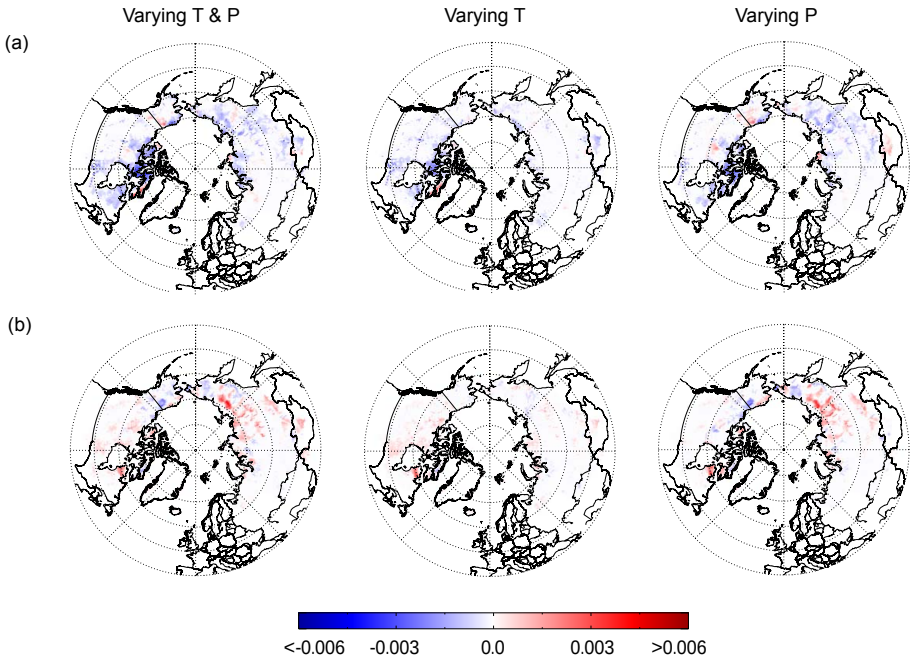

Figure 8. Similar to Fig. 7, but for simulated trends (unit: yr^{-1}) of warm-season (May–October) R_h (soil heterotrophic respiration) contribution from surface (**a**: 0–0.2 m) and deep (**b**: 0.5–3.0 m) soil carbon pools for the three experiments of the sensitivity analysis based on different configuration of surface meteorology (i.e. varying temperature T and precipitation P inputs) from 1982 to 2010.

BGD
12, 11113–11157, 2015

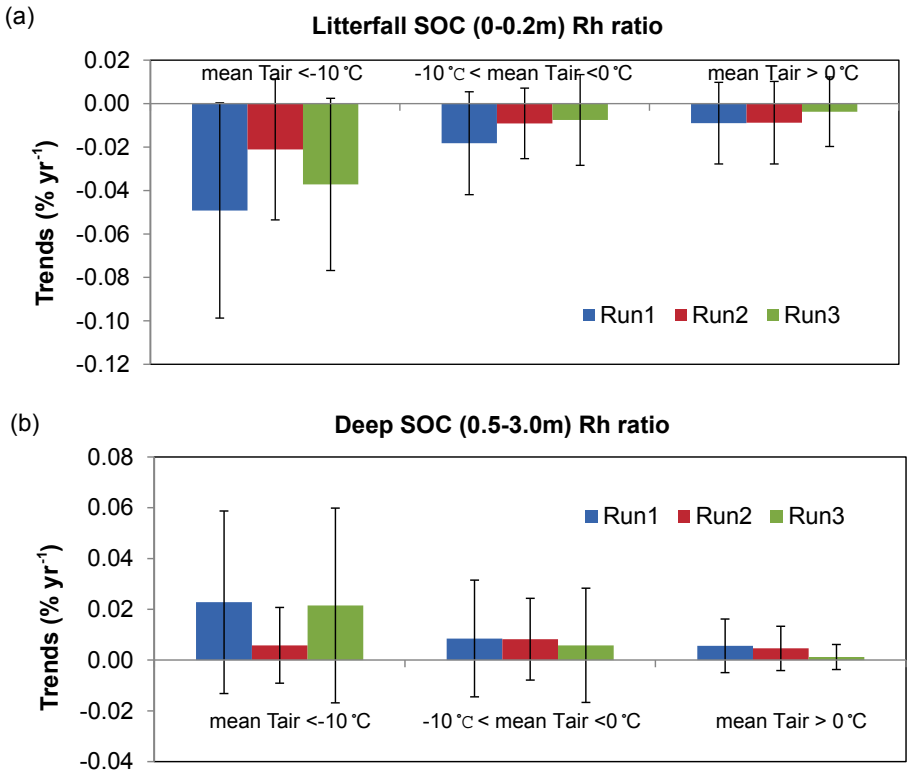

Figure 9. The zonal-average trends of warm-season (May–October) R_h (soil heterotrophic respiration) contribution from surface litterfall (0–0.2 m) and deep (0.5–3.0 m) soil carbon pools (i.e. R_h ratio) for the three experiments of sensitivity analysis from 1982 to 2010. Run1 indicates the model simulations based on varying temperature (T) and precipitation (P) inputs; Run2 indicates the model simulations based on varying T inputs alone; and Run3 indicates the model simulations based on varying P inputs alone.

BGD
12, 11113–11157, 2015